PRELIMINARY REPORT

TESTS ON CORES FROM THE WAIRAKEI GEOTHERMAL PROJECT, WAIRAKEI, NEW ZEALAND

by

R. R. Hendrickson

Submitted to

Systems, Science and Software, Inc.
Box 1620
La Jolla, California 92038

Systems, Science and Software, Inc.
Contract #S-4959 under National Science Foundation grant
AER75-14492

TR 75-63
November 1975

DISTRIBUTION OF THIS DOCUMENT IS UNLIMITED

DISCLAIMER

This report was prepared as an account of work sponsored by an agency of the United States Government. Neither the United States Government nor any agency Thereof, nor any of their employees, makes any warranty, express or implied, or assumes any legal liability or responsibility for the accuracy, completeness, or usefulness of any information, apparatus, product, or process disclosed, or represents that its use would not infringe privately owned rights. Reference herein to any specific commercial product, process, or service by trade name, trademark, manufacturer, or otherwise does not necessarily constitute or imply its endorsement, recommendation, or favoring by the United States Government or any agency thereof. The views and opinions of authors expressed herein do not necessarily state or reflect those of the United States Government or any agency thereof.

DISCLAIMER

Portions of this document may be illegible in electronic image products. Images are produced from the best available original document.

FOREWORD

This report describes testing performed by Terra Tek, Inc. for Systems, Science, and Software, Inc., of La Jolla, California. The data will be used to predict subsidence at geothermal sites. This preliminary report covers the first phase of Terra Tek's efforts under Systems, Science and Software, Inc., Purchase Order #S-4959, "Testing, Wairakei Cores". The work remaining will be started pending directions from S^3, based on the data in this report.

This page intentionally left blank.

TABLE OF CONTENTS

This page intentionally left blank.

LIST OF ILLUSTRATIONS

LIST OF TABLES

This page intentionally left blank.

INTRODUCTION

Terra Tek has conducted a series of tests on cores taken from the Wairakei geothermal site in New Zealand. The cores tested are representative of each of the four basic rock types significant to the functioning of the geothermal site. The underlying rock layer is a welded tuff known as Wairakei Ignimbrite.[1] It is the most dense of the four layers, with a saturated density of 2.36 Mg/m^3, and is relatively impermeable, thus forming a lower barrier for the aquifer. The aquifer is a tuff which is referred to as the Waiora Formation.[1] Permeability of this rock is surprisingly low, less than 50 microdarcies and it is believed that water travels primarily through fractures in the stratum. Above the aquifer is an impervious layer of mudstone known as Huka Falls Formation[1] (saturated density 1.99 Mg/m^3). The surface layer is Pumice[1] (1.88 Mg/m^3, saturated) which may serve as a thermal insulator, but is probably not necessary to the functioning of the geothermal site.

Ultrasonic velocity measurements were made for each rock type to determine elastic moduli under simulated *in situ* conditions. The Ignimbrite was found to be about four times stiffer than the Waiora Formation. Similarly, the Waiora Formation is stiffer than the Huka Formation, which is about twice as stiff as the Pumice.

Hydrostatic and triaxial deformation tests were performed on three samples of the aquifer rock to determine the effect of *in situ* stress on the elastic deformation moduli. Results show the ultrasonically determined moduli to be a factor of two to four times the deformation moduli, in agreement with other published data on porous materials.

The Waiora Formation's linear coefficient of thermal expansion was found to be 8.2×10^{-6} m/m/K, and the dry specific heat 0.17 to 0.18 cal/g-K. Thermal conductivity was measured on all four rock types (saturated) and found to decrease in stratographic order. Pumice thermal conductivity was measured at 1.03 Watts/m-K, while the Ignimbrite was 2.11 Watts/m-K.

The report that follows includes tabulation and graphical representation of the measured properties. All test procedures and apparatuses are described in detail.

It should be noted that all samples were received dry and have been out of the ground for about ten years. The effects of such a drying and resaturating cycle should be considered by the reader. In addition, the Huka Falls and Pumice cores were difficult to prepare and test, especially when saturated, as they tended to slake. However, Terra Tek was able to complete all tests as described.

Sample Identification

All samples are from a shipment of cores received by Terra Tek on August 29, 1975, shipped directly from Wairakei under the direction of Mr. W. B. Stilwell, and Mr. E.L.D. Fooks, Ministry of Works and Development, Wairakei, N.Z. The following specific bores and depths were selected for testing, based on decisions made during the meeting between Dr. Sabod Garg of S^3, and Terra Tek personnel in September, 1975.

A. Pumice, Bore hole #34, depth 134 ft.

B. Huka Falls Formation, Bore hole #37, 700 ft. to 720 ft.

C. Waiora Formation, bore hole #37, 1130 ft. to 1135 ft, hereafter referred to as "Waiora 1130 ft."

D. Waiora Formation, bore hole #37, 2296 ft. to 2618 ft., hereafter referred to as "Waiora 2618 ft."

E. Wairakei Ignimbrite, bore hole #24, 2482 ft. depth.

It should be noted that all of the material designated above was exhausted during testing, and alternate depths may have to be selected for future tests.

This page intentionally left blank.

MINERAL ANALYSIS

Mineral composition was determined by microscopic examination of standard .03 mm thin sections of the sample materials. This thickness is standard in the geological field since the constituent minerals are more readily differentiated. The first step in the analysis was the identification of as many mineral types as possible. Next, a count of the major constituents was made using a microscope reticle as a guide; 200 points were used in the count. Both plane-polarized light and cross-polarized light* were used; in both cases the light was transmitted through the thin sections.

Pumice

The pumice tested, Figure 1, is a porous, medium-grained grayish-brown rock showing banding of light and dark minerals and/or rock fragments.

Composition

	% by volume
Matrix material & voids	43
Rock fragments	24
Feldspars	17
Altered Mafic minerals	6
Pyroxenes	3
Opaques	3
Quartz	2
Amphiboles	2

*In Cross-Polarized illumination, plane-polarized light passes through the sample then through a second polarizer at right-angles to the first. Thus the only visible light is that which has been "rotated" by minerals in the sample.

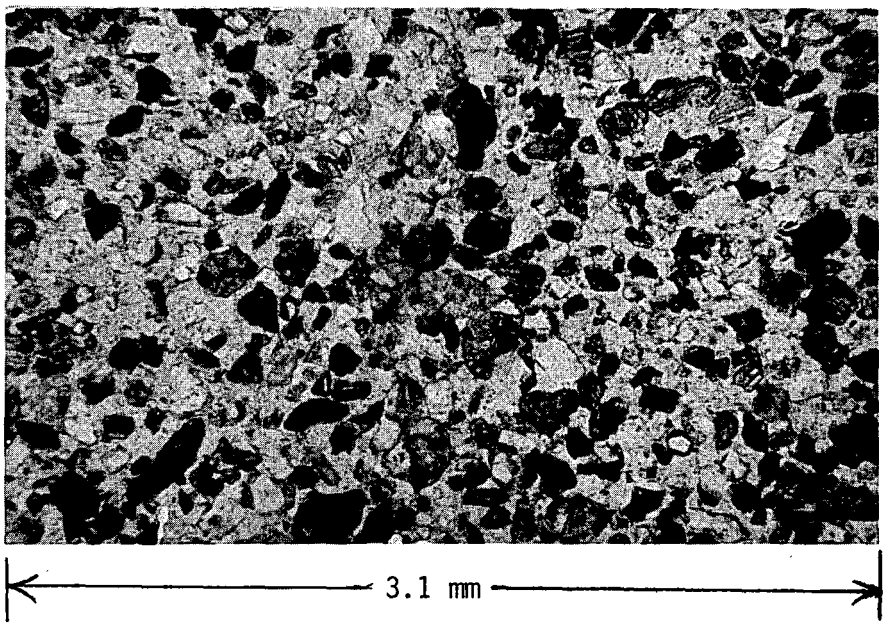

Figure 1. Pumice, Bore 34, 134', standard thin section photo, 31.25 X magnification using plane-polarized light.

Huka Falls Formation

The Huka Falls Formation Sample, Figure 2, is a fine-grained light grayish-brown mudstone. No bedding or fissility is noted. The mineral analysis revealed fine-grained clay and silt.

Composition

	% by volume
Clay .005 mm or less	86
Silt .05 mm to .005 mm	14

Waiora Formation, 1130'

This sample of the Waiora Formation is a whitish-green altered tuff with a dominant, fine-grained glassy matrix and phenocrysts of feldspar. The photo, Figure 3, shows that both the matrix and feldspars have been extensively altered. The hand specimen is chalky in appearance.

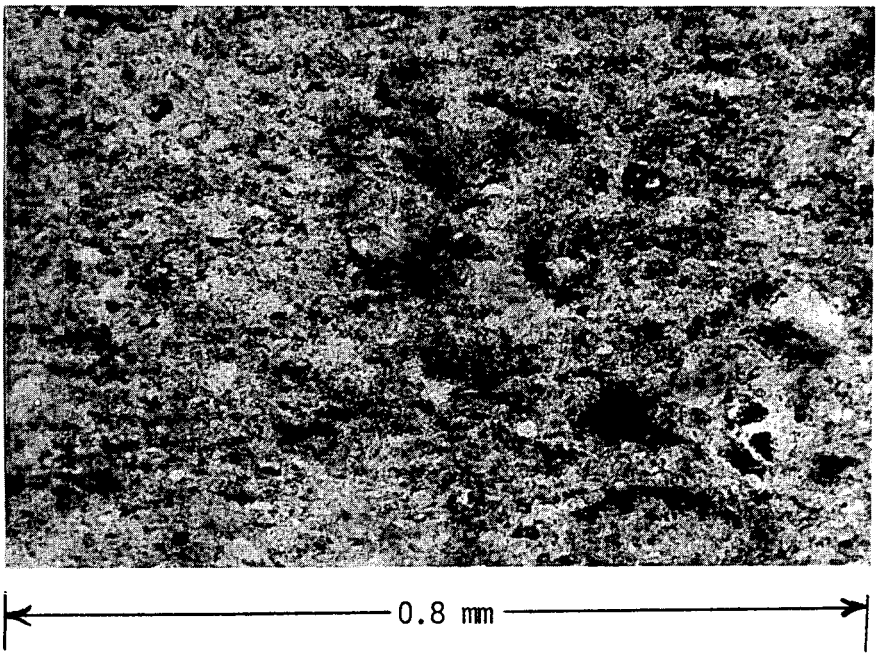

Figure 2. Huka Falls (Mudstone), Bore 37, 700', magnified X 125, plane-polarized light.

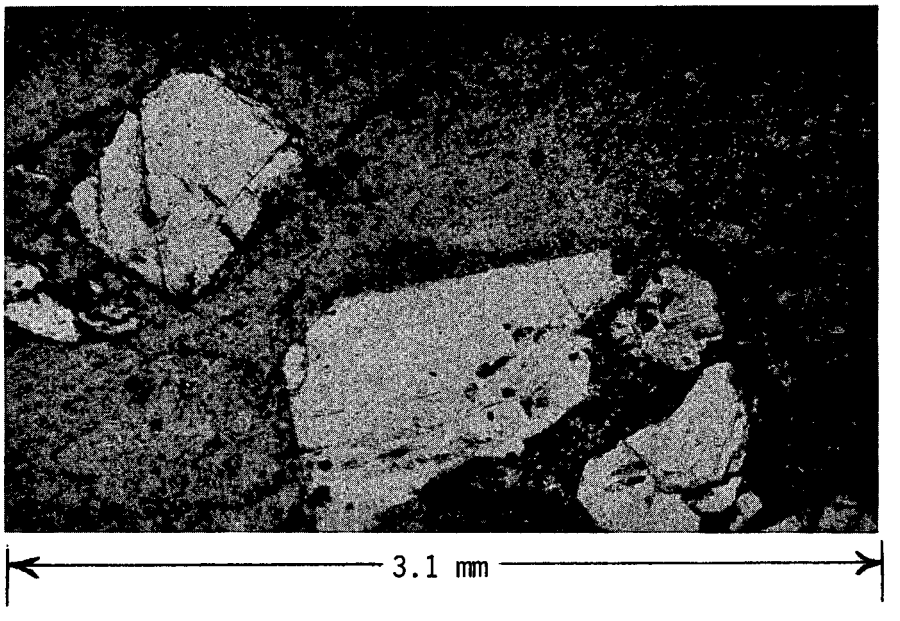

Figure 3. Waiora Formation, Bore 37, 1130', magnification 31.25 X, plane-polarized light.

Composition

	% by volume
Matrix Material	63
Feldspars	35
Opaques	2
Zeolites	Trace

Waiora Formation, 2618'

This sample of the Waiora Formation, Figure 4 is a light-brown altered tuff with a fine-grained matrix consisting of glass, quartz, feldspar and large fragments of altered mafic material. The feldspar fragments have been at least partially altered to a clay.

Composition

	% by volume
Fine-grain glassy matrix	82
Voids	14
Feldspars	2
Quartz	2
Opaques	Trace

Wairakei Ignimbrite

This Ignimbrite, Figure 5, is a grayish-green welded tuff with a fine-grained matrix of glass, quartz, feldspar and phenocrysts of glassy quartz. Some minor alteration has occurred.

Composition

	% by volume
Fine-grain matrix (glass dust)	50
Feldspar	32
Sericite	9
Quartz	5
Calcite	2
Fiberous zeolites & chlorites	2
Opaques	Trace

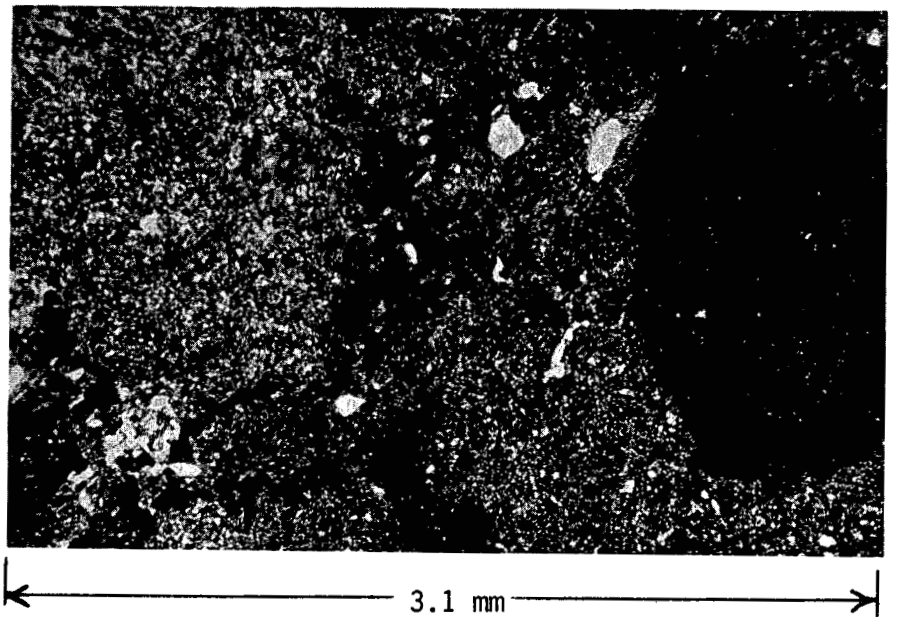

Figure 4. Waiora Formation, Bore 37, 2618', standard thin-section magnified 31.25 X, cross-polarized light.

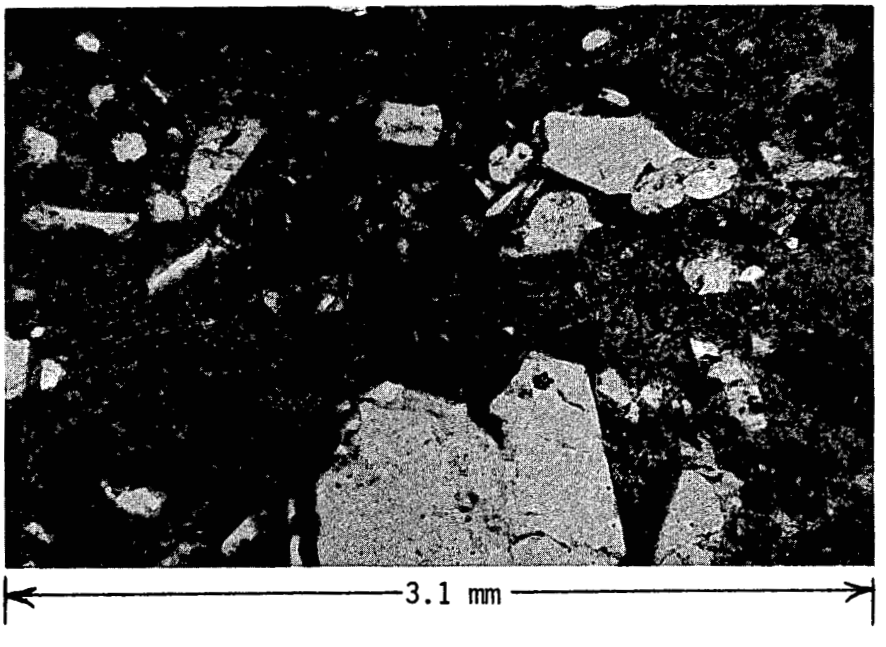

Figure 5. Wairakei Ignimbrite, Bore 24, 2482', standard thin-section photo, magnification 31.25 X, plane-polarized light.

Comments on the Lithology

The Wairakei geothermal region was created by active volcanism and rock strata are hence highly transitional both vertically and horizontally. This is confirmed by the Drill Log for the area[1].

Although a complete geotechnical analysis of the field is beyond the scope of this report, it is safe to assume that transitions between strata are generally abrupt.

PHYSICAL PROPERTIES

Dry and Saturated Bulk Densities

The bulk volume of the sample was determined by the Archimedean principle. The sample was first saturated in distilled water and weighed in the air. Next, the sample was weighed while submerged in distilled water; the difference in measured weights represents the weight of water displaced. The water temperature and pressure were measured and the corresponding water density was found from a handbook. The weight difference was then divided by the water density to yield the sample bulk volume. The sample was then dried for 24 hours at 105°C (ASTM standard procedure), allowed to cool in a desiccator, then weighed. This dry weight was then divided by the sample volume to obtain the dry bulk density. Similarly, the weight of the saturated sample in air divided by the sample bulk volume yielded the saturated bulk density. Results are listed in Table 1.

Effective Porosity

Effective porosity is the percentage of the sample volume occupied by connected pores. The volume of connected pores was determined by dividing the difference between the sample's saturated weight and its dry weight by the density of the distilled water. The volume of connected pores was then divided by sample volume to yield effective porosity. Table 1 lists the effective porosities.

Grain Density

The dried sample mentioned above was then pulverized to a 100 mesh[+] particle size for determination of grain density. The volume of the pul-

[+] U.S. Standard seive series, 0.15 mm openings, Tyler equivalent 100 mesh.

verized rock was measured using a Beckman Gas Pycnometer; grain density is the weight of the sample material divided by the measured grain volume, and is listed in Table 1.

TABLE 1

Saturated and Dry Bulk Densities, Effective Porosity, and Grain Density

ROCK TYPE	BULK DENSITY † SATURATED Mg/m^3	DRY Mg/m^3	EFFECTIVE POROSITY PERCENT BY VOLUME	GRAIN DENSITY † Mg/m^3
PUMICE	1.88	1.39	48.8 ± 0.5	2.71
HUKA FALLS	1.97	1.56	40.7 "	2.70
HUKA FALLS*	2.01	1.62	39.0 "	-
WAIORA 1130	2.01	1.59	41.6 "	2.76
WAIORA 1130*	2.04	1.65	39.1 "	-
WAIORA 1130*	2.07	1.69	37.9 "	-
WAIORA 2618*	1.99	1.64	35.6 "	2.68
WAIORA 2618*	1.99	1.60	39.1 "	-
IGNIMBRITE	2.34	2.20	13.8 "	2.69
IGNIMBRITE*	2.38	2.23	15.0 "	-

* Indicates different samples from same footage.

† Bulk density and Grain density measurements are accurate to within ± .005 Mg/m^3.

ULTRASONIC MEASUREMENTS

The technique used to measure the ultrasonic velocities is the "Through Transmission System" shown in block diagram form in Figure 6. This is an adaptation of the technique introduced by Mattaboni and Schreiber[2], and is capable of measuring small elapsed times to a high degree of accuracy. The time measurement is derived from the frequency of a very stable frequency synthesizer (stability ±1 part in 10^7/month, accuracy ±0.001 percent).

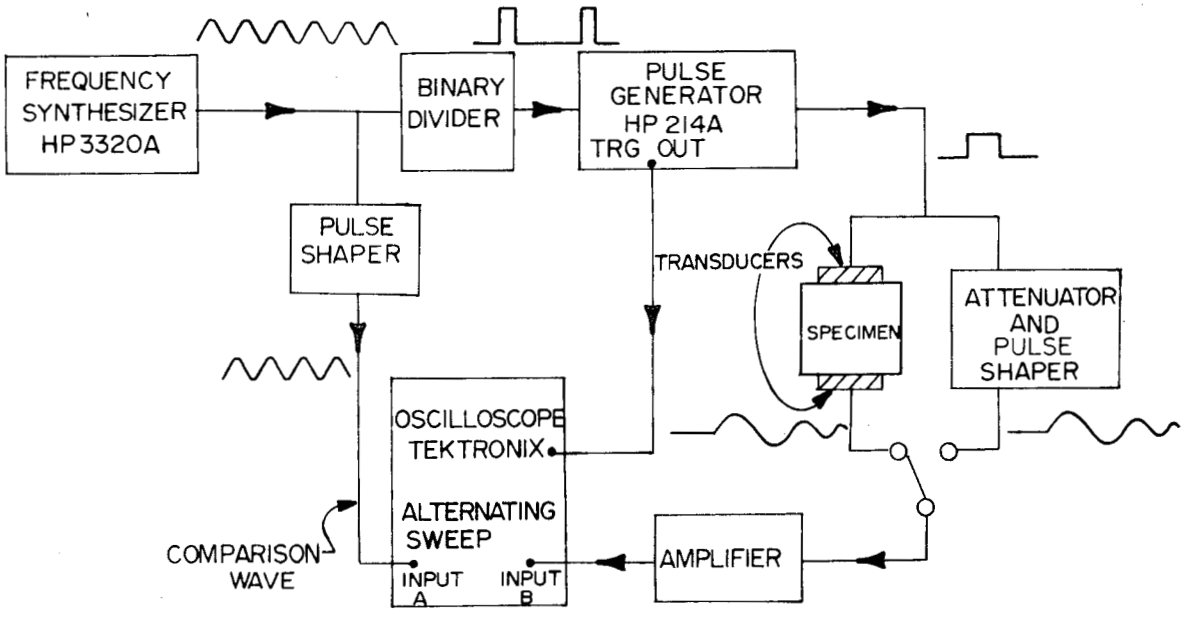

Figure 6. Through-Transmission System

The signal passing through the specimen is viewed on an oscilloscope alternately with the signal from the variable frequency synthesizer (comparison wave). The latter is modified by a pulse shaper to exactly match the wave which has passed through the specimen. Next, the pulse which excites the transmitting transducer is viewed, and its shape matched to that of the comparison wave. Once the pulse shapes are matched, they can be

made to coincide on the oscilloscope to a high degree of precision. The frequency of the synthesizer is then adjusted for an exact number of cycles between the transmitted signal and the signal through the specimen. The transit time of the ultrasonic wave through the material is obtained by dividing the number of cycles by the frequency. The binary divider is required in order to operate the pulse generator at a repetition rate that allows all of the ultrasonic wave energy to dissipate between pulses. This requires that the oscilloscope be triggered from the pulse generator in order to maintain the proper display.

Referring to Figure 7, the upper traces show the initial transmitted signal matched to the comparison wave. The lower traces (via a double-exposure) show the same comparison wave matched to the signal that passed through the specimen. In this example there were twelve cycles of comparison wave between the initial signal and the signal through the specimen. The

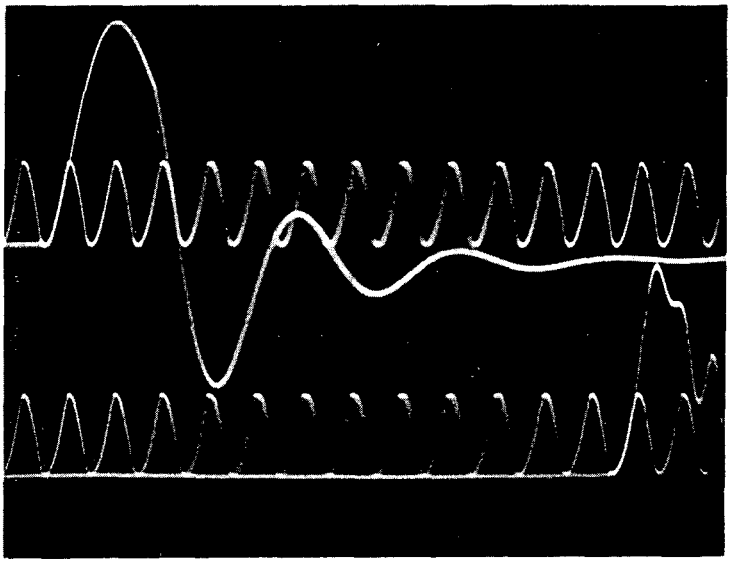

Figure 7. Oscilliscope display showing the comparison wave and the signal through a specimen in the lower trace and the comparison wave and the initial signal in the upper trace.

frequency synthesizer setting was 0.3542 MHz, the elapsed time was therefore 33.879 μsec. Because of the difference in the inherent delay in the electrical and acoustic paths, it is necessary to determine a time correction using a reference sample. The velocity of the acoustic wave in the specimen is obtained by dividing the path length by the corrected elapsed time.

Derivation of Moduli from Ultrasonic Velocity Measurements

The following classic relationships were used to calculate moduli from ultrasonic velocity measurements.

V_s = Shear-wave velocity, km/sec ± 1%

V_p = Plane-wave velocity, km/sec ± 1%

ρ = Density, Mg/m^3 ± 0.005 Mg/m^3

A. Young's Modulus, E

$$E = \frac{3\rho\ V_s^2\ (V_p^2 - 4/3\ V_s^2)}{V_p^2 - V_s^2}\ , \text{GPa}$$

B. Bulk Modulus, K

$$K = \rho\ (V_p^2 - 4/3\ V_s^2)\ , \text{GPa}$$

C. Shear Modulus, G

$$G = \rho V_s^2\ , \text{GPa}$$

D. Poisson's Ratio, ν

$$\nu = \frac{E - 2G}{2G} = \frac{V_p^2/2 - V_s^2}{V_p^2 - V_s^2}$$

E. Constrained Modulus, B

$$B = \rho\ V_p^2\ , \text{GPa}$$

Ultrasonic Data and Calculated Moduli

The following are the ultrasonically determined velocities and calculated elastic moduli. The designation "P-Wave" represents the longitudinal wave, while "S-Wave" stands for the shear wave. Sample density is found in the "Physical Properties" section. Each test was performed at hydrostatic confining pressures selected to simulate the range of *in situ* stress.

Pumice, 134'

Density: 1.36 Mg/m^3, dry

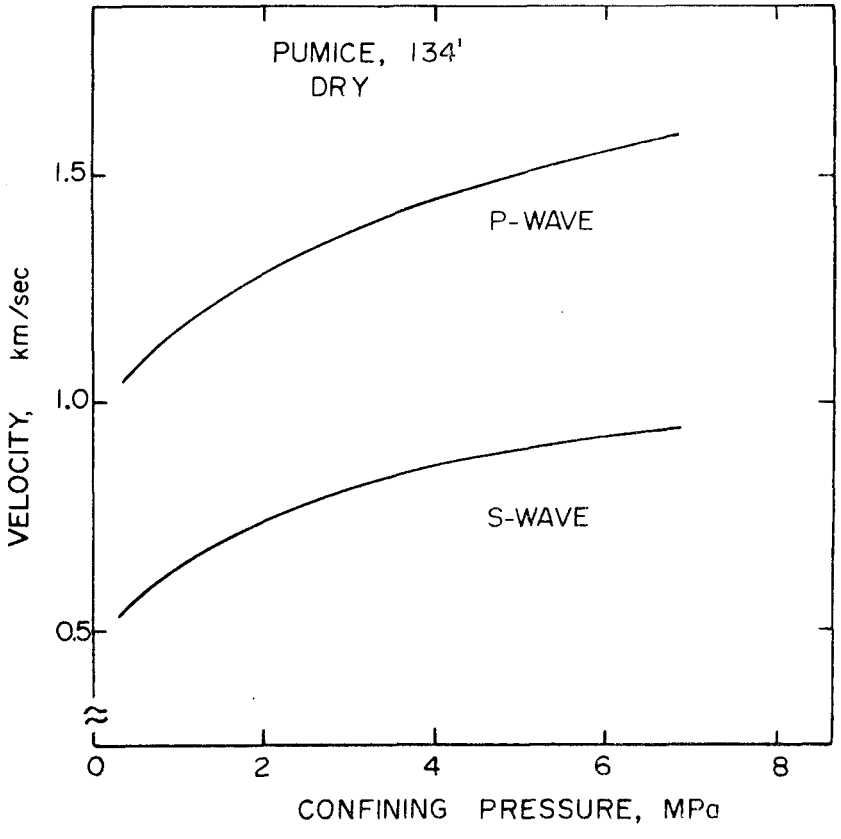

Figure 8. Longitudinal and Shear-wave velocities vs. Confining pressure in Pumice, 134'.

TABLE 2

Pumice, 134', Velocities and Moduli at Five Confining Pressures

CONFINING PRESSURE MPa	VELOCITIES P-WAVE Km/sec	S-WAVE Km/sec	POISSON'S RATIO	MODULI CONSTR. GPa	SHEAR GPa	BULK GPa	YOUNG'S GPa
.35	1.05	.532	.328	1.50	.385	.989	1.02
.69	1.17	.560	.332	1.70	.427	1.13	1.14
3.45	1.39	.827	.225	2.62	.930	1.38	2.28
5.52	1.51	.910	.215	3.10	1.13	1.60	2.74
6.89	1.58	.942	.224	3.40	1.21	1.79	2.96

Huka Falls Formation, 700'

Density: 1.605 Mg/m^3, dry

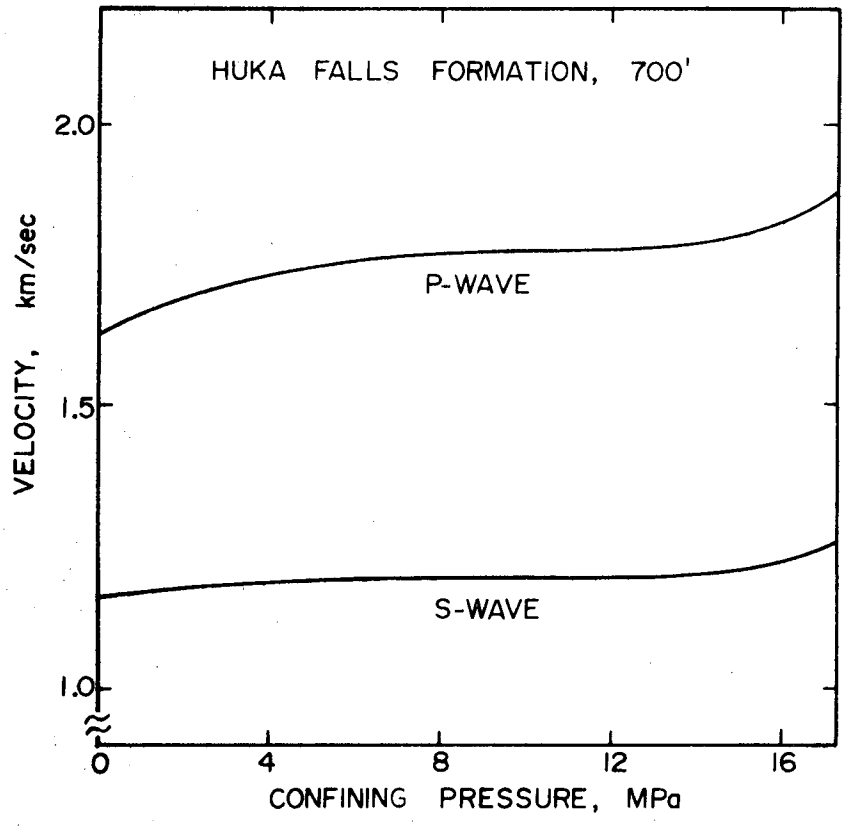

Figure 9. Longitudinal and Shear-wave velocities vs. confining pressure in Huka Falls Formation, 700'.

TABLE 3

Huka Falls Formation, 700', Velocities and Moduli at Six Confining Pressures

CONFINING PRESSURE MPa	VELOCITIES P-WAVE Km/sec	S-WAVE Km/sec	POISSON'S RATIO	MODULI CONSTR. GPa	SHEAR GPa	BULK GPa	YOUNG'S GPa
0	1.64	1.17	≈0	4.31	2.21	1.36	4.30
3.45	1.73	1.18	.062	4.81	2.25	1.81	4.77
6.89	1.77	1.20	.070	5.02	2.32	1.93	4.96
10.34	1.77	1.19	.081	5.02	2.29	1.97	4.95
13.79	1.80	1.20	.104	5.19	2.29	2.13	5.06
17.24	1.88	1.25	.107	5.66	2.49	2.34	5.52

The increase in wave velocity above about 14 MPa is considered to be due to pore-collapse; this material is a mudstone and is substantially weaker than the other rocks tested.

Waiora Formation, 2618'

Density: 2.00 Mg/m^3, water saturated

TABLE 4

Waiora Formation, 2618', Velocities and Moduli at Seven Confining Pressures

CONFINING PRESSURE MPa	VELOCITIES P-WAVE Km/sec	S-WAVE Km/sec	POISSON'S RATIO	MODULI CONSTR. GPa	SHEAR GPa	BULK GPa	YOUNG's GPa
0	2.22	1.08	.344	9.85	2.34	6.73	6.29
3.45	2.46	1.23	.333	12.1	3.02	8.05	8.06
6.89	2.59	1.31	.329	13.4	3.41	8.82	9.07
10.34	2.63	1.34	.324	13.9	3.60	9.06	9.54
13.79	2.66	1.37	.321	14.1	3.73	9.16	9.85
17.24	2.69	1.38	.322	14.5	3.79	9.40	10.0
20.95	2.71	1.39	.322	14.6	3.84	9.52	10.1

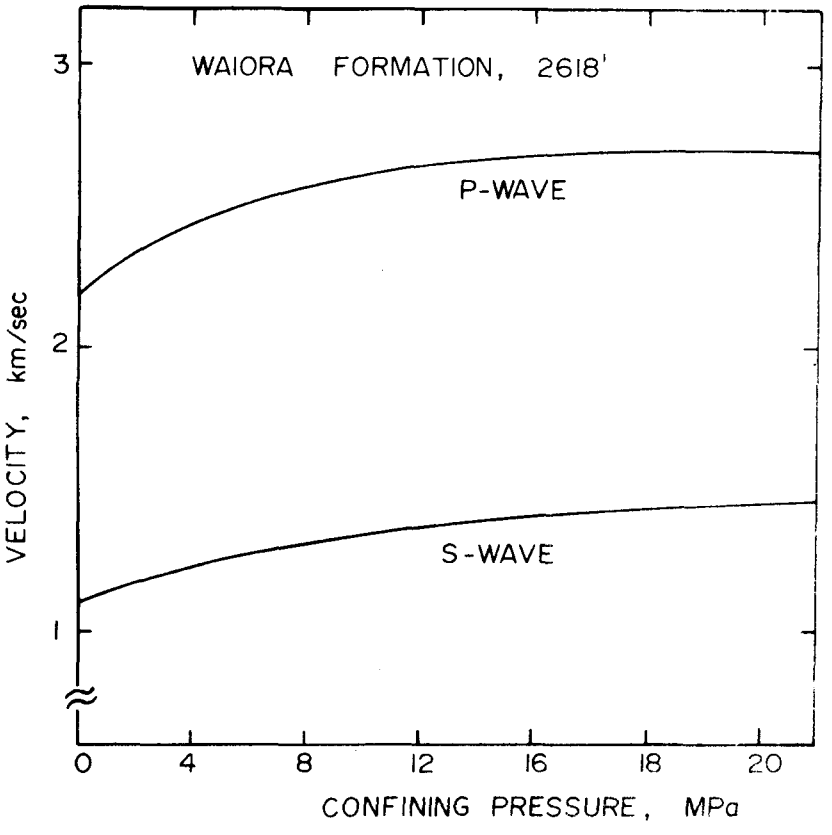

Figure 10. Longitudinal and Shear-Wave Velocities vs. confining pressure in Waiora Formation, 2618'.

Wairakei Ignimbrite, 2482'

Density: 2.33 Mg/m^3, water saturated

TABLE 5

Wairakei Ignimbrite, 2482', Velocities and Moduli at Six Confining Pressures

CONFINING PRESSURE MPa	VELOCITIES P-WAVE Km/sec	S-WAVE Km/sec	POISSON'S RATIO	MODULI CONSTR. GPa	SHEAR GPa	BULK GPa	YOUNG'S GPa
0	4.22	2.52	.223	41.6	14.8	21.8	36.2
3.45	4.25	2.54	.221	42.1	15.1	22.0	36.8
6.89	4.30	2.57	.223	43.1	15.4	22.6	37.6
10.34	4.33	2.59	.222	43.8	15.6	22.9	38.2
13.79	4.36	2.61	.222	44.3	15.8	23.2	38.6
17.24	4.38	2.62	.222	44.6	16.0	23.4	39.0

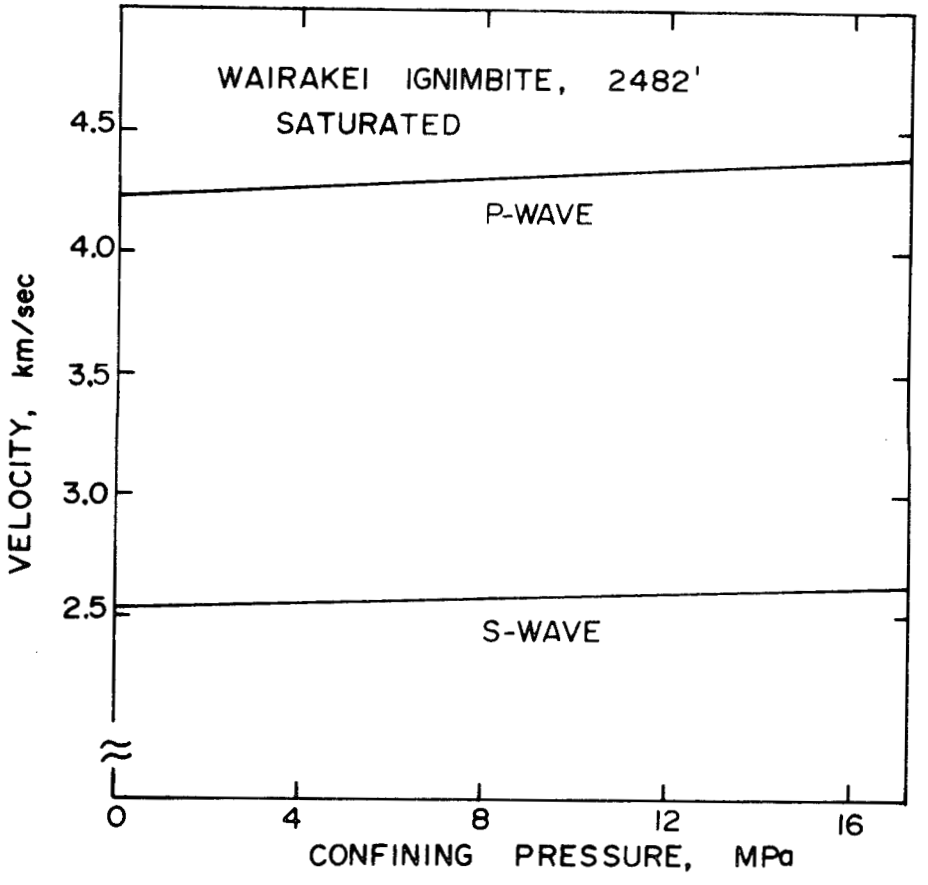

Figure 11. Longitudinal and shear-wave velocities vs. confining pressure in Wairakei Ignimbrite, 2482'.

PERMEABILITY MEASUREMENT

Permeability can be measured or estimated by any one of several different methods. Typical laboratory determinations of permeability, however, are usually made using one of the following two methods:

1. The constant flow or steady-state method which uses a flow meter or positive displacement pump to measure or control the flow rate through the sample. This method requires the flow rate through the material and the pressure drop across the material to be a constant at the time of measurement.
2. The transient method which imposes a small step of differential pressure in a known volume on one side of sample. The permeability can be calculated from the time-dependent decay of this imposed pressure step.

Each method has advantages and disadvantages depending on the conditions required for the test and the permeability of the sample in question. The constant flow method is well documented and is widely used for porous media having permeabilities greater than 100 μd. The second method is more suitable for low porosity materials such as tight sandstones where the permeabilities are in terms of microdarcies.[3]

Figure 12 illustrates the apparatus used by Terra Tek for making permeability tests with the transient method. The sample is placed in a pressure vessel and pore pressure inlet and outlet lines are connected to the external hardware. The sample can be subjected to hydrostatic pressure and/or axial loading during the permeability test. Pore pressure can be regulated to any value less than the confining pressure. As can be seen from this figure, there are volumes of fluid on either side of the sample which can be hydraulically connected to allow the pore pressure to equalize. When the sample has reached equilibrium, the volumes are disconnected by closing a valve. Referring to

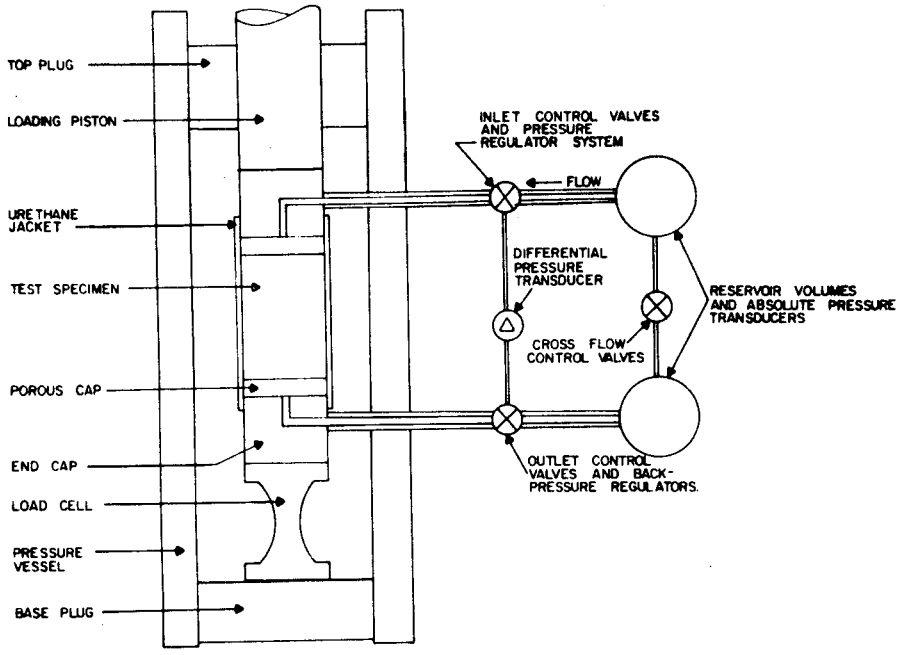

Figure 12. A sketch of the test apparatus used to measure permeability.

Figure 13, the pressure in Volume #1 is raised slightly and then applied to the sample suddenly. This pressure step is normally only a few percent of the absolute pressure in the reservoir volume. The pressure step decay is monitored accurately through the use of a differential pressure transducer. Sample length and reservoir volume can be changed to allow the test to be completed in a convenient length of time.

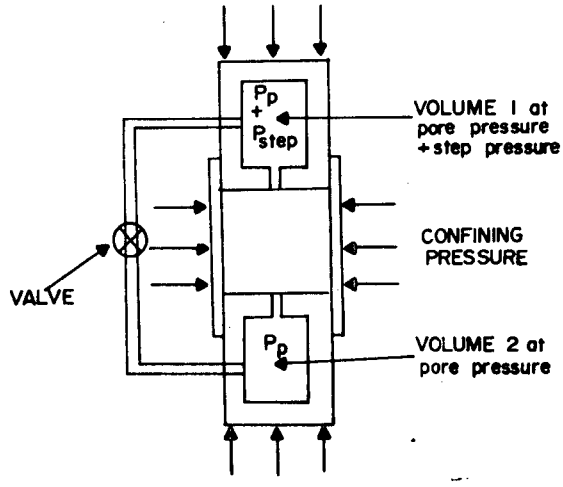

Figure 13. A schematic of a permeability test.

A brief outline of the theory involved in measuring permeabilities using the transient technique is given below. A detailed treatment of this analysis is presented in Reference 4. The equation for compressible flow in a compressible media is

$$\nabla^2 P = \frac{\mu\beta}{k} C \frac{\partial P}{\partial t} \qquad (1)$$

Where

μ = fluid viscosity

β = fluid compressibility

k = permeability

C = a term which includes the compressibility of the rock matrix

and

P = pressure

If the following assumptions are made concerning fluid flow characteristics,

1. Darcy's law is valid.
2. The fluid flow is laminar.
3. The change in fluid volume in the pores in the rock, due to the the step pressure change, is negligible compared to the amount fluid flowing through the sample during a test.
4. The pressure step is small compared to the absolute pore pressure so that the physical constants of the fluid (viscosity and compressibility) can be considered constant in all parts of the sample.

then the solution to Equation (1) is given by:

$$\Delta P = \overline{\Delta P} \left[\frac{V_2}{V_1+V_2} \right] e^{-\alpha t} \qquad (2)$$

$\overline{\Delta P}$ = Initial step pressure added

ΔP = (Instantaneous pressure) - (Final pressure) i.e., $(P-P_f)$

V_1 = volume at top of sample

V_2 = volume at bottom of sample

α = the slope of the semi-log plot of the natural log of the decaying pressure versus time.

The permeability k is given from Equation (2) as:

$$k = \frac{\alpha \beta \mu \ell}{A(1/V_1 - 1/V_2)} \qquad (3)$$

where

ℓ = the sample length

A = the sample area

Thus, the permeability can be determined with no direct measurement of the flow rate. Clearly this is a major advantage for making:

1. Accurate measurements on very tight samples.
2. Using the system at high pore pressures.

Data, Permeability vs. Effective Stress

Figure 14 is a plot of permeability in microdarcies vs. effective stress, i.e., confining pressure minus the pore pressure. Pore pressure was constant throughout the test while confining pressure was increased from 15 MPa up to 25 MPa, then decreased back to 15 MPa. As the effective stress was increased, a change in the slope of the curve was noted above 8 MPa, probably indicating the completion of micro-crack closures and/or pore collapse. As the effective stress was decreased, the sample exhibited substantially lowered porosity. This is typical of many rocks, and permeability will usually return

to the original (unconfined) value after being left unconfined for several days. Repeatability of the permeability measurements is ±5% or better.

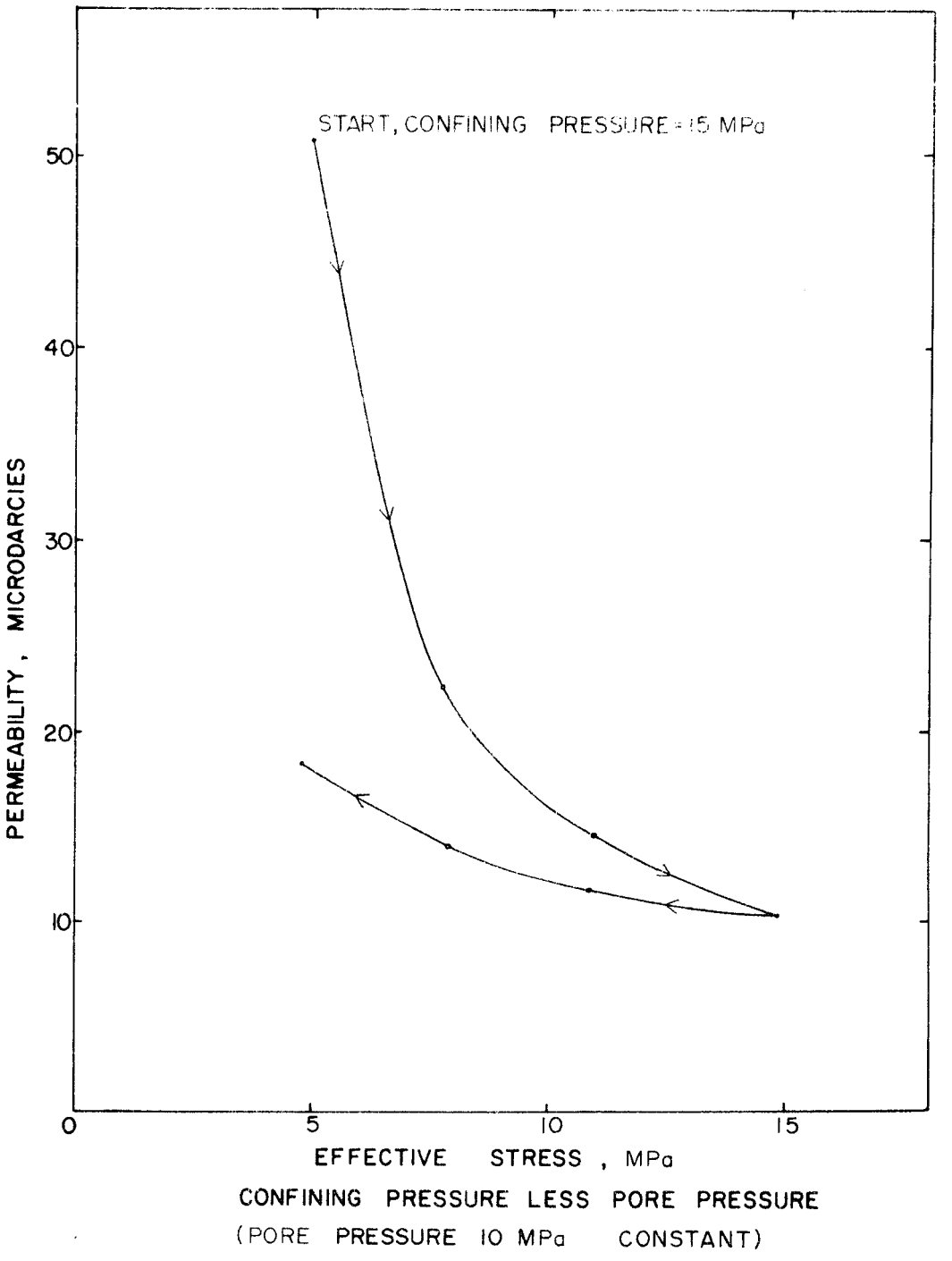

Figure 14. Waiora Formation, 1130', Permeability in Microdarcies vs. Effective Stress

This page intentionally left blank.

HYDROSTATIC & TRIAXIAL TESTS

The bulk modulus (K) and shear modulus (G) were determined with hydrostatic and triaxial loading tests. Prepared samples were 5.08cm diameter x 6.35 cm long; ends were ground parallel to within ± 0.025 mm. Samples were sealed in urethane jackets and mounted between steel end caps. The lower end cap permits drainage to a 50 cc pore fluid chamber within the end cap; this insures that pore pressure within the sample is zero. Figure 15 depicts the test hardware. Confining pressure (p) was monitored with both a diaphragm pressure transducer and a Heise pressure gauge (bourdon tube mechanism), having a resolution of ±70 kPa.

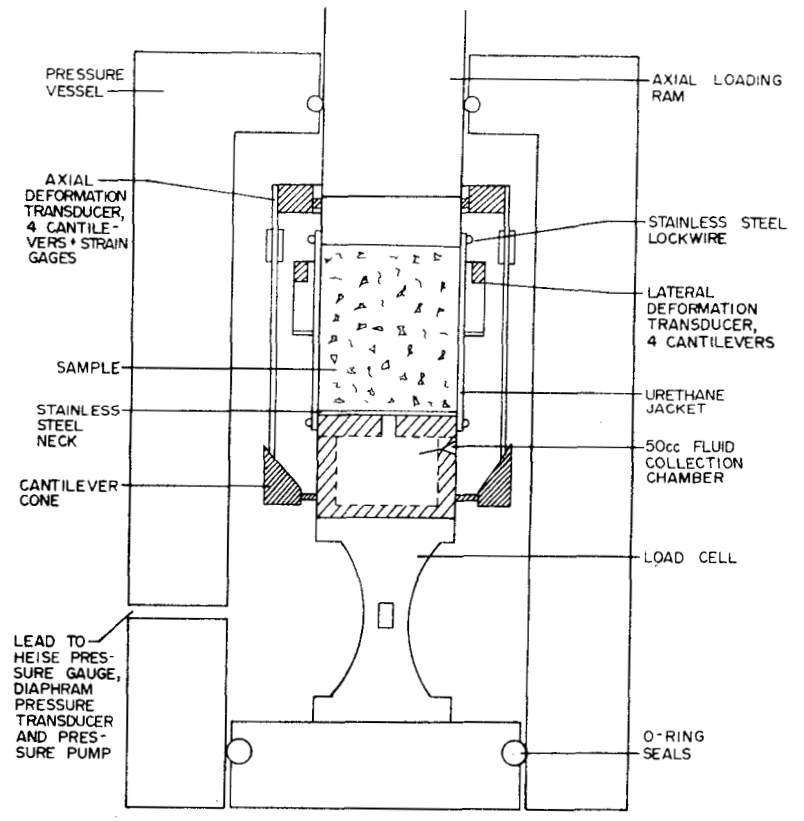

Figure 15. Hydrostatic and Triaxial Test Apparatus

The axial load (L) was measured with a load cell located within the pressure vessel. Axial strain is measured via four cantilever arms mounted on a steel ring, and spaced 90^{o} apart. These cantilevers slide on a 30^{o} cone mounted to the other end of the sample. The strain-gauge bridge is wired such that effects of sample tilting, if any exists, will not affect the measurement. Resolution of this system is ±0.025% strain. Transverse strain was measured using another strain-gauge bridge consisting of four cantilevers mounted to a free-floating ring. The cantilevers contact the urethane jacket at the sample midpoint. Deformation of the urethane due to confining pressure is extremely small but is well known and has been taken out of the data. Similarly, the effect of hydraulic pressure on the strain gauges used in the load cell and cantilevers is removed by a computer program during the data reduction process. Resolution of the Transverse strain cantilever system is ± 0.02% strain. Both cantilever systems were recalibrated prior to use.

The first step in the experimental procedure was the application of confining pressure (3.5 MPa) with axial and lateral strains being recorded. Next, an axial load was applied with confining pressure constant. The axial load was limited to about 75 percent of the materials's ultimate strength; this value was estimated from the shape of the resultant stress-strain plot. The axial load was then removed and the confining pressure increased to 10.4 MPa, followed by a second axial loading and unloading. Finally, the confining pressure was increased to 17.2 MPa, followed by axial loading up to the yield point. Figure 16 illustrates the stresses described. Electrical signals representing confining pressure, lateral strain, axial strain, and axial load were recorded on XY plotters.

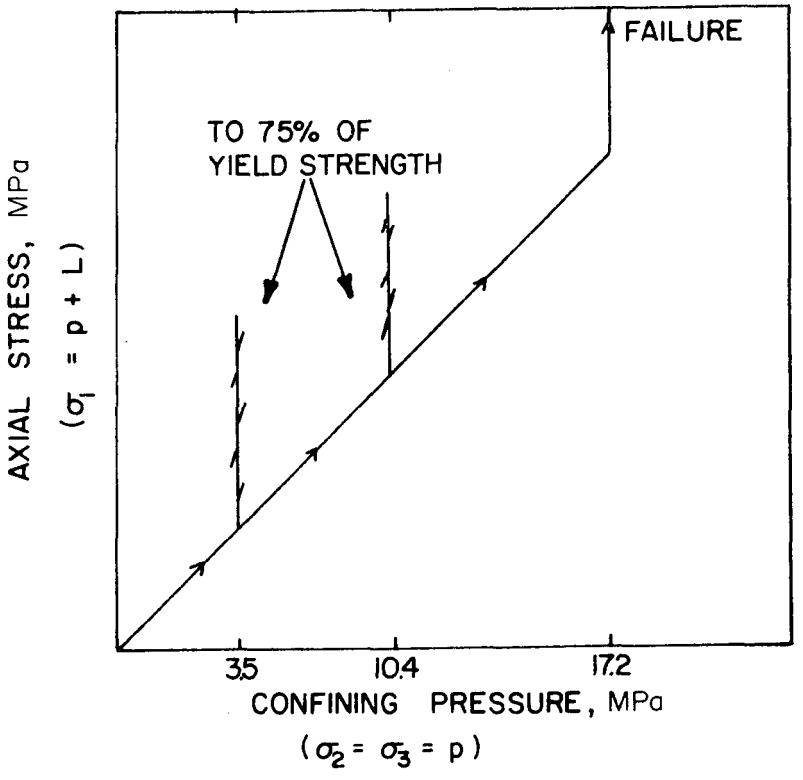

Figure 16. Triaxial Loading Schedule

Bulk Modulus

The bulk modulus is defined as

$$K = \frac{\Delta P \cdot V}{\Delta V} = \frac{\Delta P}{\varepsilon_1 + \varepsilon_2 + \varepsilon_3} \text{ , GPa}$$

where

V = sample volume

ε_1 = axial strain due to confining pressure (cantilever & cone system)

$\varepsilon_2 = \varepsilon_3$ = average lateral strain due to confining pressure (floating cantilevers)

ΔP = Increase in confining pressure, GPa

Poisson's Ratio, ν

The Poisson's ratio is derived from the ratio of average lateral strain to the axial strain:

$$\nu = \frac{\varepsilon_{2,3}}{\varepsilon_1}$$

Young's Modulus, E

E is derived directly from the plot of differential stress vs. axial strain, with the confining pressure held constant. Table 7 lists the Moduli measured for each confining pressure; see Figures 18 and 19.

Shear Modulus, G

G is derived from previously calculated functions:

$$G = \frac{E}{2\ (1+\nu)}$$

Results of Hydrostatic and Triaxial tests

Table 6 presents the hydrostatic test results, Figure 17 is the plot of mean stress vs. volume strain from which the bulk moduli of Table 6 were derived.

TABLE 6

Bulk Modulus Measurements for Three Samples of Waiora Formation Over Three Regions of Confining Pressure

SAMPLE IDENTIFICATION	CONFINING PRESSURE, MPa	BULK MODULUS GPa ±0.13 GPa
WAIORA, 1130'	0 to 3.5	0.41
	3.5 to 10.4	2.03
	10.4 to 17.2	1.70
WAIORA 2618', #1	0 to 3.5	0.69
WAIORA 2618', #2	0 to 3.5	0.73
	3.5 to 10.4	1.98
	10.4 to 17.2	2.86

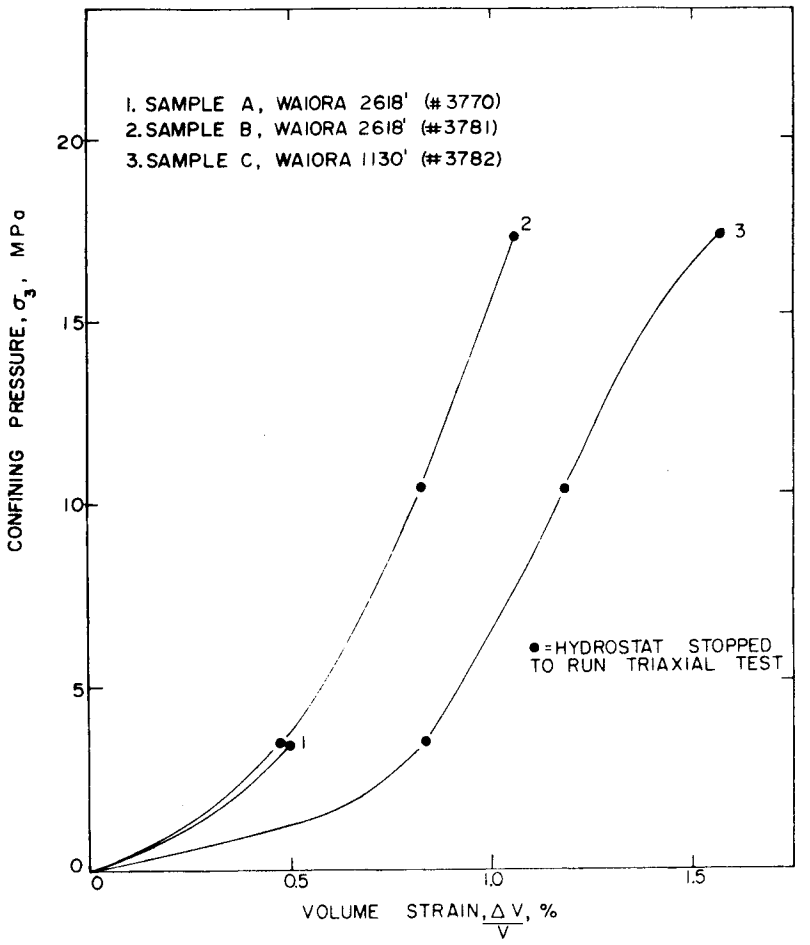

Figure 17. Mean Stress, MPa, vs. Volume Strain, Percent.

TABLE 7

Young's Modulus, Poisson's Ratio, and Shear Modulus for Three Samples of Waiora Formation at Three Confining Pressures

SAMPLE IDENTIFICATION	CONFINING PRESSURE MPa	YOUNG'S MODULUS GPa, ± .18 GPa	POISSON'S RATIO ±0.04	SHEAR MODULUS GPa ± 0.15 GPa
WAIORA, 1130'	3.5	0.91	0.21	0.38
	10.4	1.48	0.24	0.60
	17.2	1.75	0.22	0.72
WAIORA, 2618'#1	3.5	2.65	0.11	1.19
WAIORA, 2618'#2	3.5	2.90	0.12	1.30
	10.4	4.20	0.15	1.82
	17.2	4.94	0.23	1.99

Figure 18 shows plots of differential stress vs. axial strain (quadrant I) and vs. lateral strain (quadrant II) for a sample of the Waiora Formation from the 1130-foot level. Three separate confining pressures were used. Figure 19 is a similar plot for two samples from the 2618-foot level of the Waiora Formation. Table 7 is a presentation of the moduli derived from the graphs shown in Figures 18 and 19.

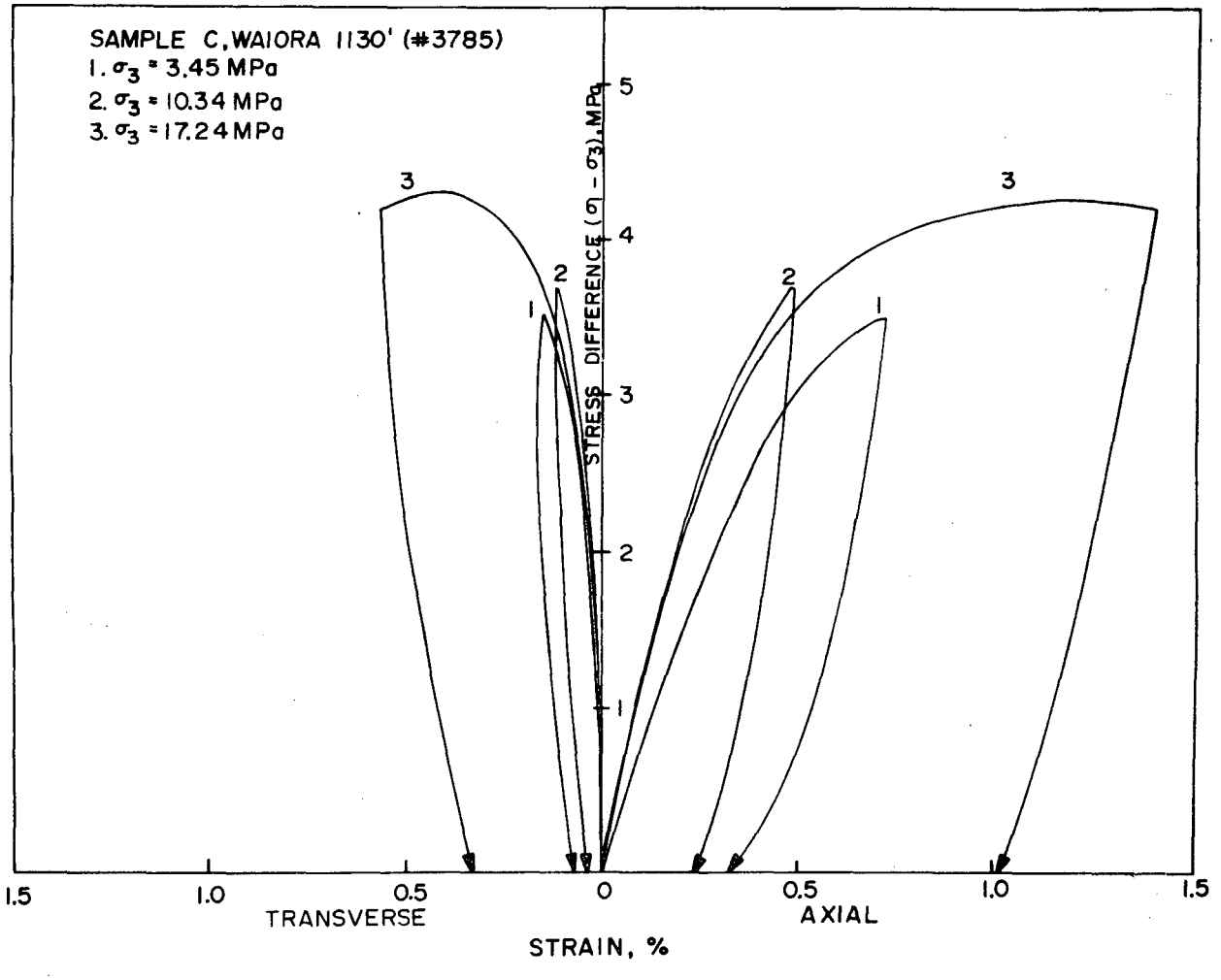

Figure 18. Differential Stress vs. Axial Strain and vs. Lateral Strain in Waiora Formation, 1130'.

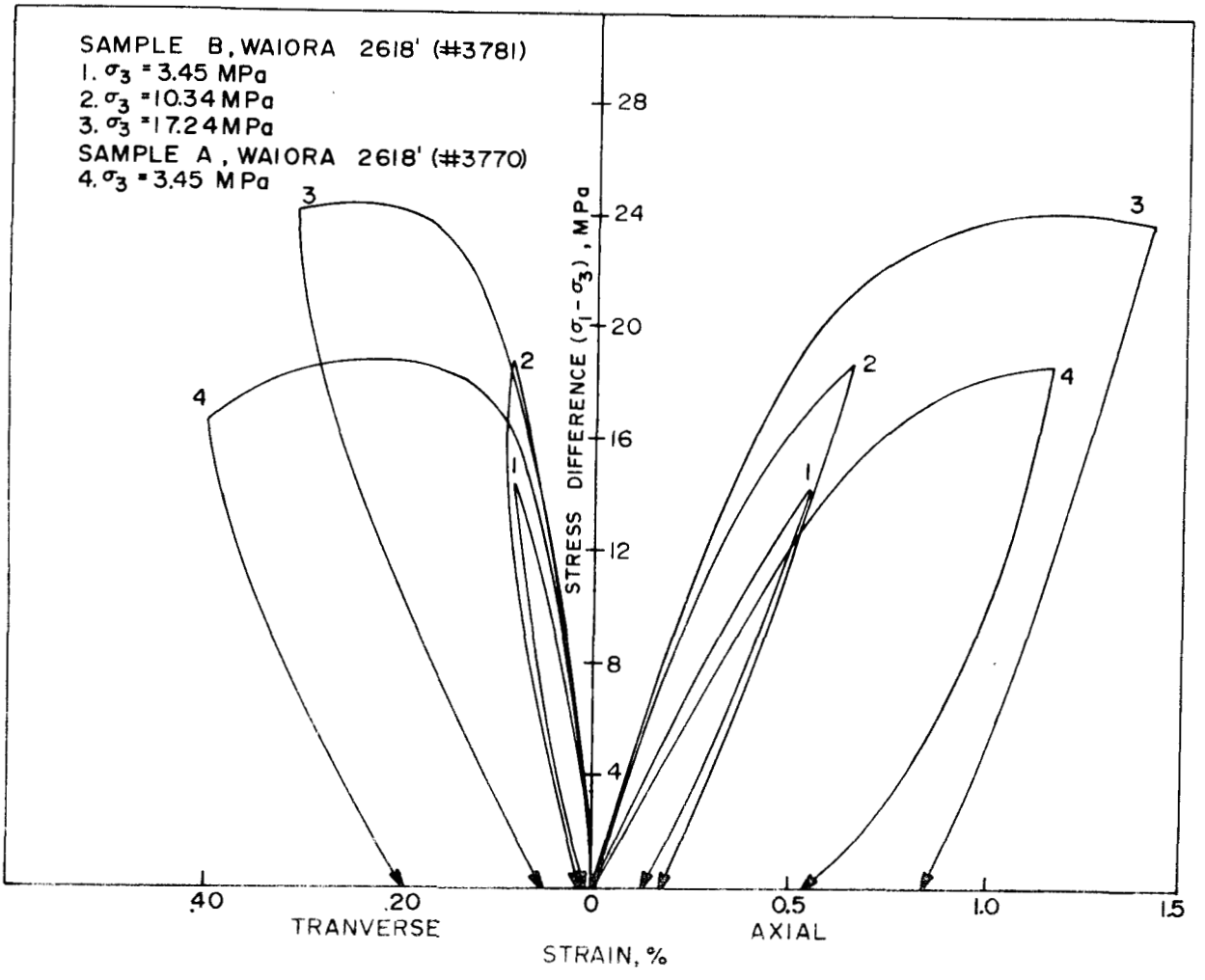

Figure 19. Differential Stress vs. Axial Strain and vs. Lateral Strain in Two Samples of Waiora Formation, 2618'.

Comparison With Ultrasonic Measurements

The four moduli for Waiora 2618' found by deformation measurements were also determined via ultrasonic velocity measurements on another sample from the same footage. The ultrasonic data yields stiffer moduli than those found by deformation tests. While this is atypical for competent materials, it is typical for porous or less competent rocks. Discrepencies of this sort normally show ultrasonic moduli from two to four times greater than those found by deformation tests. Terra Tek is presently investigating the basis of these discrepencies.

This page intentionally left blank.

LINEAR COEFFICIENT OF THERMAL EXPANSION, α

Figure 20 illustrates the equipment used to measure the coefficient of linear expansion. Two linear variable differential transformers (LVDT's) are used to monitor expansion of the sample. The sample is 2.5 cm diameter by 5.1 cm long, and has a thermocouple bonded to it for accurate monitoring of sample temperature. The slight error introduced by expansion of the fused quartz rods running the length of the sample is calculated out of the data. The remainder of each quartz rod is enclosed in a quartz tube, and expansion

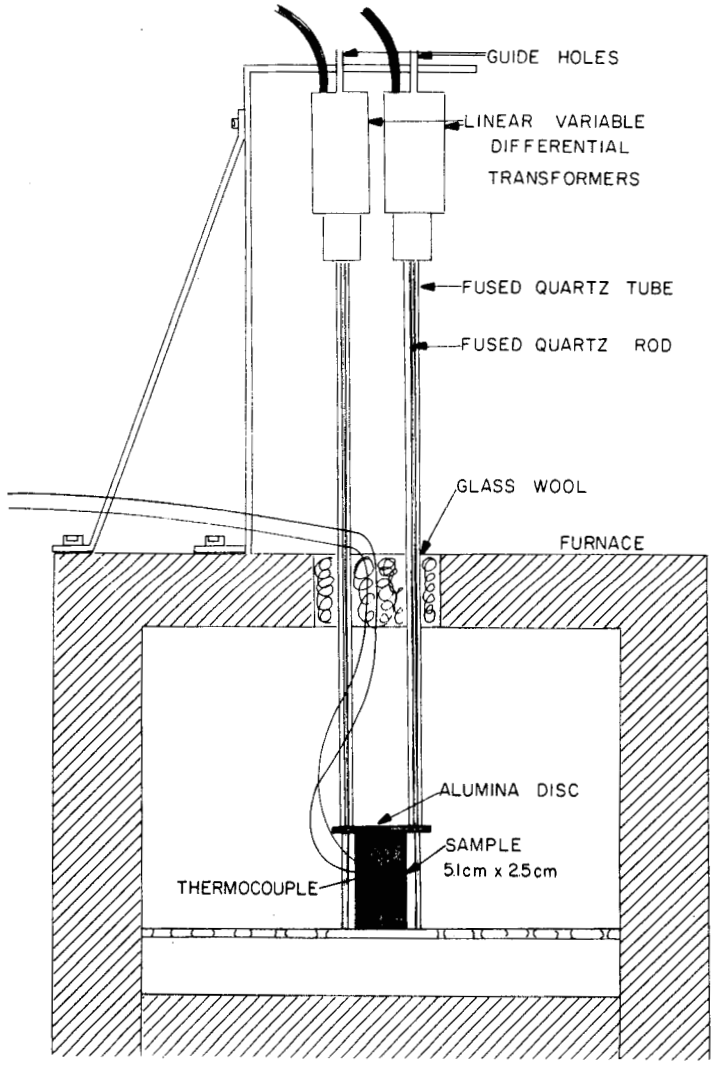

Figure 20. Measurement of Linear Coefficient of Thermal Expansion

effects are cancelled. The experiment is allowed to stabilize for an hour after the furnace reaches the desired temperature.

Data: Linear Coefficient of Thermal Expansion

Sample:	Waiora 1130', dry
length:	5.1 cm
dia:	2.5 cm
cold temp:	$22^{o}C$
hot temp:	$238^{o}C$
ΔT:	$216^{o}C$

$$\alpha = 8.2 \times 10^{-6} \text{ m/m/K} \pm 5\%$$

SPECIFIC HEAT MEASUREMENT

Figure 21 depicts the apparatus used to determine the specific heat of a sample. An aluminum calorimeter of known heat capacity is embedded in rigid polyurethane foam at least 10 cm thick in all directions. The calorimeter separates into upper and lower halves for loading of the sample. The sample material is contained in a cylindrical low-mass aluminum container having very flat ends.

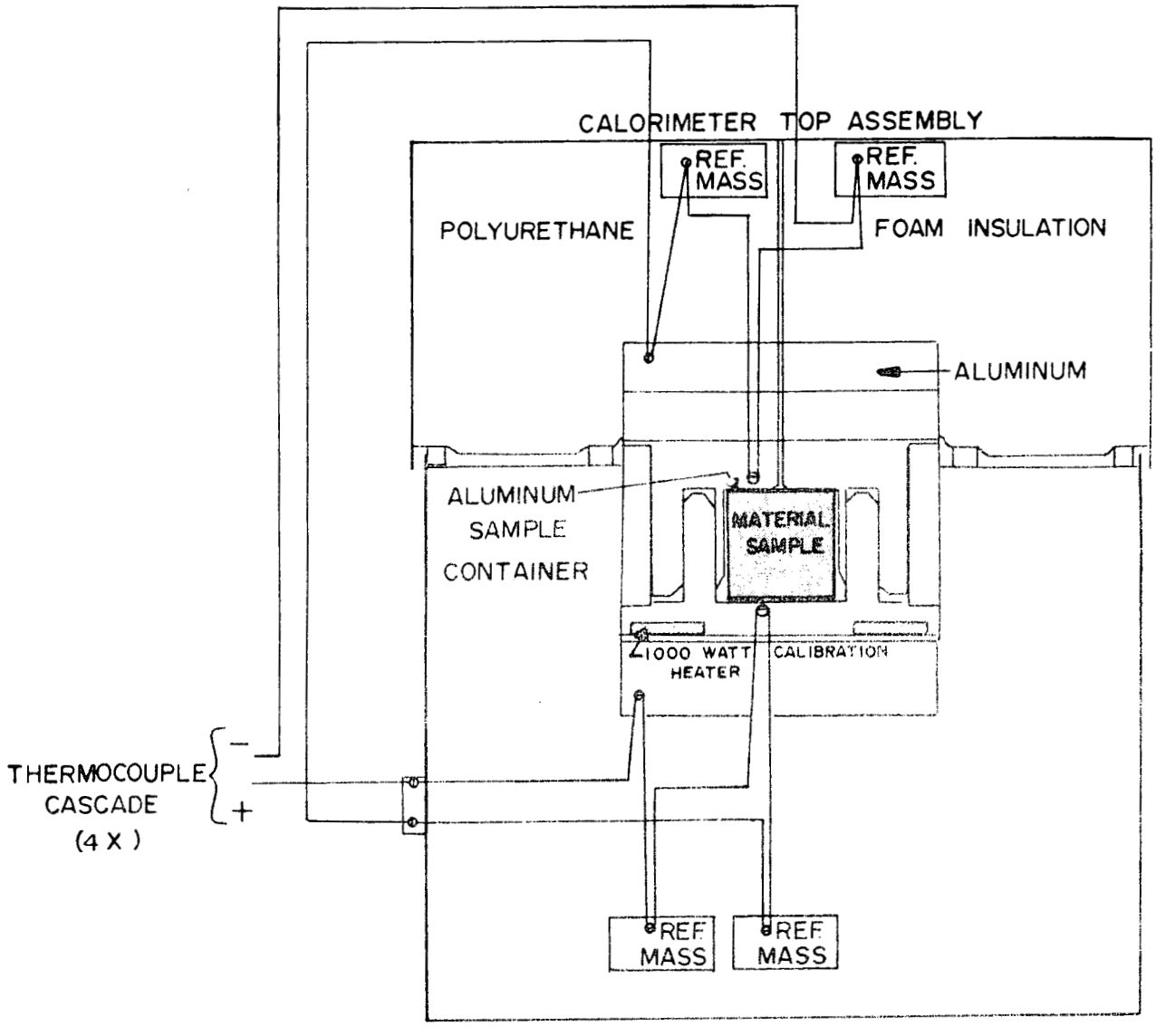

Figure 21. Calorimeter System

The sample (5.1 cm dia. x 5.1 cm long) has precision-ground flat ends, ±.0025mm, to facilitate heat transfer to the calorimeter. Temperature rise of the calorimeter is measured via an X4 thermocouple cascade driving an instrumentation amplifier having a gain of 1000. Thus temperature rises can easily be measured with a resolution of ±.001 K. Calibration of the calorimeter is accomplished by means of a built-in electric heater.

The current, voltage and duration of the heating provide the caloric input figure and when combined with the temperature rise, provide the heat capacity. A slight amount of heat will, however, escape into the insulation. This is corrected for as follows: First, the calibration heating rate is tailored to be similar to the rate of transfer of heat from the sample (found by a preliminary test). Secondly, the temperature rise of the calorimeter is not measured until after the temperature has peaked. The time of the reading is fixed and is the same for both the calibration and the actual testing. This effectively compensates for any heat loss to the insulation.

The sample material is located within the aluminum sample container, and heated to the desired temperature in an oven. Temperature is monitored via a thermocouple located directly on the sample container. The sample container is situated within a heavy iron vessel in the oven during the heating process. The iron vessel is used to transfer the aluminum carrier and sample to the calorimeter without heat loss. Calorimeter loading can be accomplished within 5 seconds or less.

Calculation of Specific Heat, c

By definition,[5] the average specific heat between two temperatures is:

$$c = \frac{Q}{m(T_1-T_2)} = \frac{Q}{m\Delta T}$$

where

Q = heat, calories (4.185 joule/cal)
T_1 = initial temperature, K
T_2 = final temperature, K
m = mass of sample, g

The average specific heat of the sample, c_s, is therefore:

$$c_s = \frac{Q_c}{m_s \Delta T_s} = \frac{\text{calories}}{\text{gm-K}}$$

where

Q_c = heat delivered to calorimeter by the sample, cal.
ΔT_s = temperature drop of sample, K
m_s = sample mass, g

and

$$Q_c = C_c \Delta T_c - C_a \Delta T_s$$

C_c = heat capacity of calorimeter, cal/K
ΔT_c = temperature rise of calorimeter, K
C_a = heat capacity of (aluminum) sample carrier, cal/K

Table 8, below lists the specific heat results on two samples of the aquifer stratum, the Waiora Formation.

TABLE 8

Specific Heat for Waiora 1130' and 2618'

Rock Type	Specific Heat cal/g-K	T-Initial ^oC	T-Final ^oC	ΔT ^oC
Waiora 1130'	0.174 ±10%	232.2	32.8	199.4
Waiora 2618'	0.180 ±10%	231.5	33.6	197.9

This page intentionally left blank.

THERMAL CONDUCTIVITY

Figure 22 illustrates the thermal conductivity measurement apparatus. The test requires all electrical power supplied to the sample heater to escape through the sample. To insure that this takes place, the sample heater is surrounded by a copper guard cup. The temperature of the guard heater is held constant by a fully proportional electronic temperature control. The sample heater is held to within ±.05K of the guard cup by means of an X4 thermocouple cascade driving a high-gain amplifier which controls power to the sample heater. The space between the two heaters contains

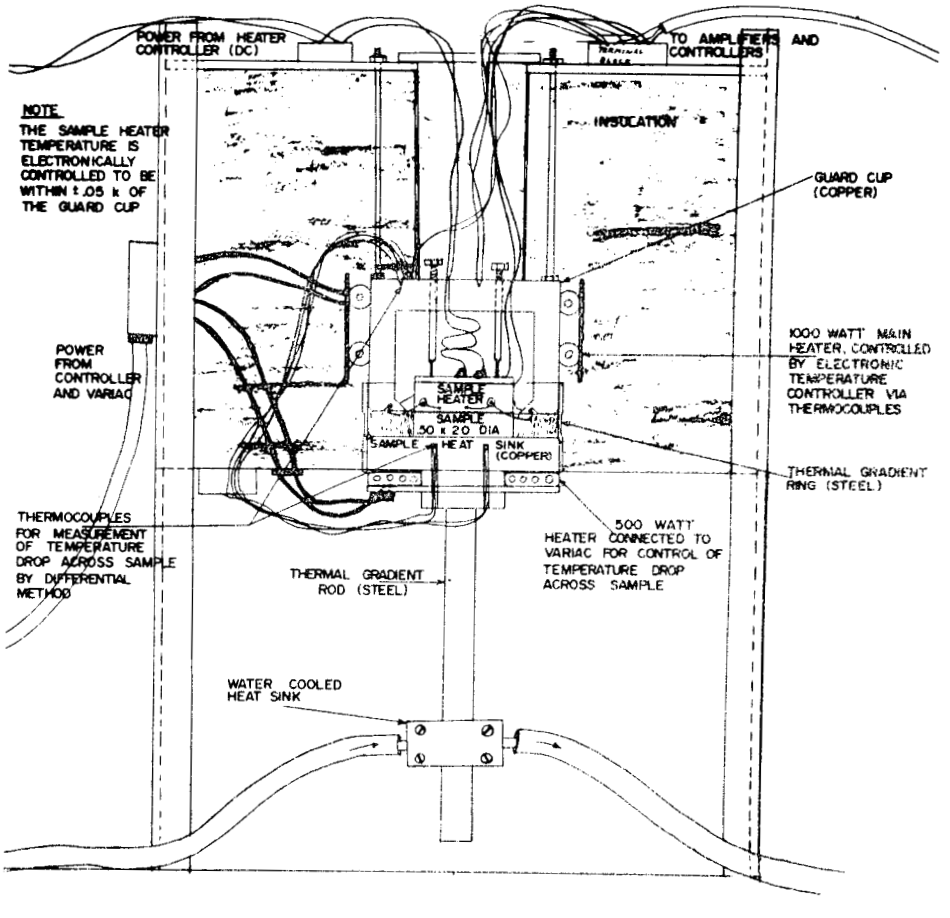

Figure 22. Thermal Conductivity Experiment

loosely packed glass wool.

Heat flows out of the experiment to a water-cooled heat sink. The heat sink can be moved up and down the "thermal gradient rod" to regulate the temperature drop across the sample. Water cooling and electronic control of the guard-cup heater insure rapid thermal stabilization throughout the experiment.

In order to insure that there is no heat transfer through the sides of the sample, it is surrounded with insulation contained by the "thermal gradient ring". Since this insulation sees an identical vertical temperature gradient on the edge of the sample and on the inside surface of the "thermal gradient ring", there will be no lateral heat flow.

Temperatures of the sample top and sample bottom are determined by thermocouples embedded in the guard-cup and in the sample heat sink. Both probes are within 2.5 mm of the constant-temperature planes. This measurement system is acceptable because the thermal conductivity of copper is about 250 times that of rock. In addition, heat transfer into and out of the sample must be optimized. Both the sample heater and sample heat sink have been lapped and polished to be flat at the heat transfer surfaces. The flat faces of the sample are ground flat to within ±0.0025 mm, and three stainless steel screws apply pressure to the sample heater.

Calculation of k

$$k = \frac{P \cdot \ell}{A \cdot \Delta T} = \frac{\text{watts}}{\text{meter-kelvin}}$$

P = power, sample heater current x voltage (watts)
ΔT= top temperature - bottom temperature, K
A = sample cross-section, square meters
ℓ = sample thickness, meters

Test Procedure, Wairakei cores (saturated)

The Wairekei samples were vacuum saturated and then sealed in an aluminum foil jacket. A thin layer of thermal compound was used on both the inside and outside surfaces of the foil covering the top and bottom of the sample. Heat flow through the foil on the side of the sample was calculated and removed from the data (a correction of about 20%). Samples were weighed before and after testing to insure that the sample had not leaked. Data were taken when all readings had stabilized (about 35 minutes).

Table 9 lists the Thermal Conductivities Measured on the four basic rock types. All samples were saturated.

TABLE 9

Thermal Conductivity for Saturated Pumice 134', Huka 700', Waiora 2618' and Ignimbrite 2482'

ROCK TYPE	CONDUCTIVITY WATT/m-K	HOT FACE °C	COOL FACE °C
Pumice 134'	1.03 ±10%	81.5	46.0
Huka 700'	1.28 ±10%	82.6	49.5
Waiora 2618'	1.56 ±10%	82.5	48.8
Ignimbrite 2482'	2.11 ±10%	82.8	51.1

This page intentionally left blank.

REFERENCES

1. Drill Log, Wairakei Geothermal Field, R. W. Willett, New Zealand Geological Survey Bulletin #75.

2. P. Mattiboni and E. Schreiber, "Method of Pulse Transmission Measurements for Determining Sound Velocities," Journal of Geophysical Research,Vol. 72, No. 20, October 15, 1967.

3. L. J. Klinkenberg, "The Permeability of Porous Media to Liquids and Gasses," Am. Petrol Inst., Drilling Production Practices, 2, 200, 1942.

4. W. F. Brace, J. B. Walsh and W. T. Frangos, "Permeability of Granite under High Pressure," Journal of Geophysical Research, Vol. 73, No. 6, March, 15, 1968.

5. M. W. Zemansky, "Heat and Thermodynamics," McGraw-Hill, p. 70, 1957.

This page intentionally left blank.

ACKNOWLEDGEMENTS

I would like to thank the following Terra Tek personnel for performing experiments and providing technical descriptions of their work: Richard Dropek, basic characteristics and triaxial tests; Dr. Henri Swolfs, mineral analysis, Dick Lingle, ultrasonic measurements, and Randy Nielsen, permeability measurement. I would also like to thank Lynn Barker for consultations on the design of the thermal conductivity, specific heat and linear expansion experiments.